Computer Physics Communications 180 (2009) 1721–1729

Contents lists available at ScienceDirect

Computer Physics Communications

www.elsevier.com/locate/cpc

Numerical calculation of the reflectance of sub-wavelength structures on silicon nitride for solar cell application

Kartika Chandra Sahoo [a], Yiming Li [b,c,*], Edward Yi Chang [a]

[a] Department of Materials Science and Engineering, National Chiao Tung University, Hsinchu 300, Taiwan
[b] Department of Electrical Engineering, National Chiao Tung University, Hsinchu 300, Taiwan
[c] National Nano Device Laboratories, Hsinchu 300, Taiwan

ARTICLE INFO

Article history:
Received 2 March 2009
Received in revised form 9 April 2009
Accepted 19 April 2009
Available online 22 April 2009

Keywords:
Silicon nitride
Sub-wavelength structure
Pyramid shape
Antireflection coating
Multilayer
Rigorous coupled-wave approach
Reflectance
Efficiency
Morphological effect

ABSTRACT

In this study, we calculate the spectral reflectivity of pyramid-shaped silicon nitride (Si_3N_4) sub-wavelength structures (SWS). A multilayer rigorous coupled-wave approach is advanced to investigate the reflection properties of Si_3N_4 SWS. We examine the simulation results for single layer antireflection (SLAR) and double layer antireflection (DLAR) coatings with SWS on Si_3N_4 surface, taking into account effective reflectivity over a range of wavelengths and solar efficiency. The results of our study show that a lowest effective reflectivity of 1.77% can be obtained for the examined Si_3N_4 SWS with the height of etched part of Si_3N_4 and the thickness of non-etched layer of 150 and 70 nm, respectively, which is less than the results of an optimized 80 nm Si_3N_4 SLAR (~5.41%) and of an optimized DLAR with 80 nm Si_3N_4 and 100 nm magnesium fluoride (~5.39%). 1% cell efficiency increase is observed for the optimized Si solar cell with Si_3N_4 SWS, compared with the cell with single layer Si_3N_4 antireflection coatings (ARCs); furthermore, compared with DLAR coated solar cell, the increase is about 0.71%. The improvement on the cell efficiency is mainly due to lower reflectance of Si_3N_4 SWS over a wavelength region from 400 to 600 nm that leads to lower short circuit current.

1. Introduction

The antireflection coating is a key factor for solar cell design [1–3]. Many studies have been reported for double layer antireflection (DLAR) coatings because single layer antireflection (SLAR) coatings are not able to cover a broad range of the solar spectrum [4–8]. Unfortunately, these multilayer antireflection coatings (ARCs) are expensive to fabricate owing to the stringent requirement of high vacuum, material selection, and layer thickness control. An alternative to multilayer ARCs is the sub-wavelength structures (SWS) surface with dimensions smaller than the wavelength of light. In publications concerning broadband or solar antireflection surfaces [9–12], the principle to achieve the necessary low refractive indices is always the same: substrate material is mixed with air on a sub-wavelength scale. To date, a wide variety of techniques were examined for texturing microcrystalline-Si cells [13–16]. One of promising options is surface texturing by dry etching technique. Fabricating uniform textures with a submicron scale on mc-Si wafers by reactive ion etching (RIE) for Si solar cells [17,18] has been studied. But, this may form the dislocations and defects in the semiconductor layer. These defects and dislocations are responsible for increasing the minority carrier recombination in solar cell. Thus, the short circuit current for the solar cell is decreased, which in turn decreases the efficiency of solar cell. Also, the reflectance property of textured antireflection coatings has not been clearly drawn yet for Si solar cells. Based upon this observation, study the possibility of sub-wavelength structure on ARC surface instead of semiconductor surface may benefit the Si solar cell technologies.

In this work, we numerically study the reflectance of SWS on silicon nitride (Si_3N_4) for solar cell application. Since Si_3N_4 is a well-known ARC used in semiconductor industry, we explore the texturization on Si_3N_4 ARC and its optical properties. The main motivation behind this lies in the fact that the sub-wavelength structures will act as a second ARC layer with an effective refractive index so that the total structure can perform as a DLAR layer. Thus, we could cost down the deposition of 2nd ARCs layer can be saved with better or comparable performance as that of a DLAR solar cell. We calculate the spectral reflectivity of pyramid-shaped Si_3N_4 SWS. A multilayer rigorous coupled-wave approach (RCWA) [19–21] is advanced to investigate the reflection properties of Si_3N_4 SWS. In contrast to conventional constant refractive index expression for Si, a wavelength-dependent expression is implemented in our calculation of reflectance of Si_3N_4 SWS. We first optimize structures including Si SWS, Si_3N_4 SWS, Si_3N_4 SLAR and

* Corresponding author at: Department of Electrical Engineering, National Chiao Tung University, Hsinchu 300, Taiwan.
E-mail address: ymli@faculty.nctu.edu.tw (Y. Li).

0010-4655/$ – see front matter
doi:10.1016/j.cpc.2009.04.013

Si_3N_4/magnesium fluoride (MgF_2) DLAR for the best effective reflectance properties. Using the optimized morphologies, we further compare the simulation results of reflectance for SLAR and DLAR coatings with SWS on Si_3N_4, over a range of wavelengths. The reflectance data obtained from RCWA simulation for the optimized SWS is used in PC1D [22] to get the electrical data (e.g., short circuit current J_{SC} and open circuit voltage V_{OC}) and cell efficiency; we notice that PC1D is one of the commonly used software for solar cell modeling. The solar efficiencies obtained from PC1D simulation for SWS, SLAR coating and DLAR coating are also compared and discussed.

This paper is organized as follows. In Section 2, we brief the procedure of RCWA for the simulated single pyramidal structure including the adopted material parameters. In Section 3, we show the results and compare the main difference of reflectance among structures. Finally, we draw conclusions and suggest future work.

2. Structure and solution method

For the simplicity, a single pyramidal structure, shown in Fig. 1(a), is explored for the reflectance property with respect to the wavelength. The region with brown color of SWS is Si_3N_4, the region with sky color stands for Si substrate, and the environment of the triangular part is air. The etched Si_3N_4 (i.e., the height of triangular part) is h and the thickness of the non-etched Si_3N_4 is s, both of these two parameters are designing parameters for the reflectance optimization. The studied SWS is a diffractive structure and its reflectance property could be calculated by a rigorous coupled-wave analysis (RCWA) technique. RCWA is an exact

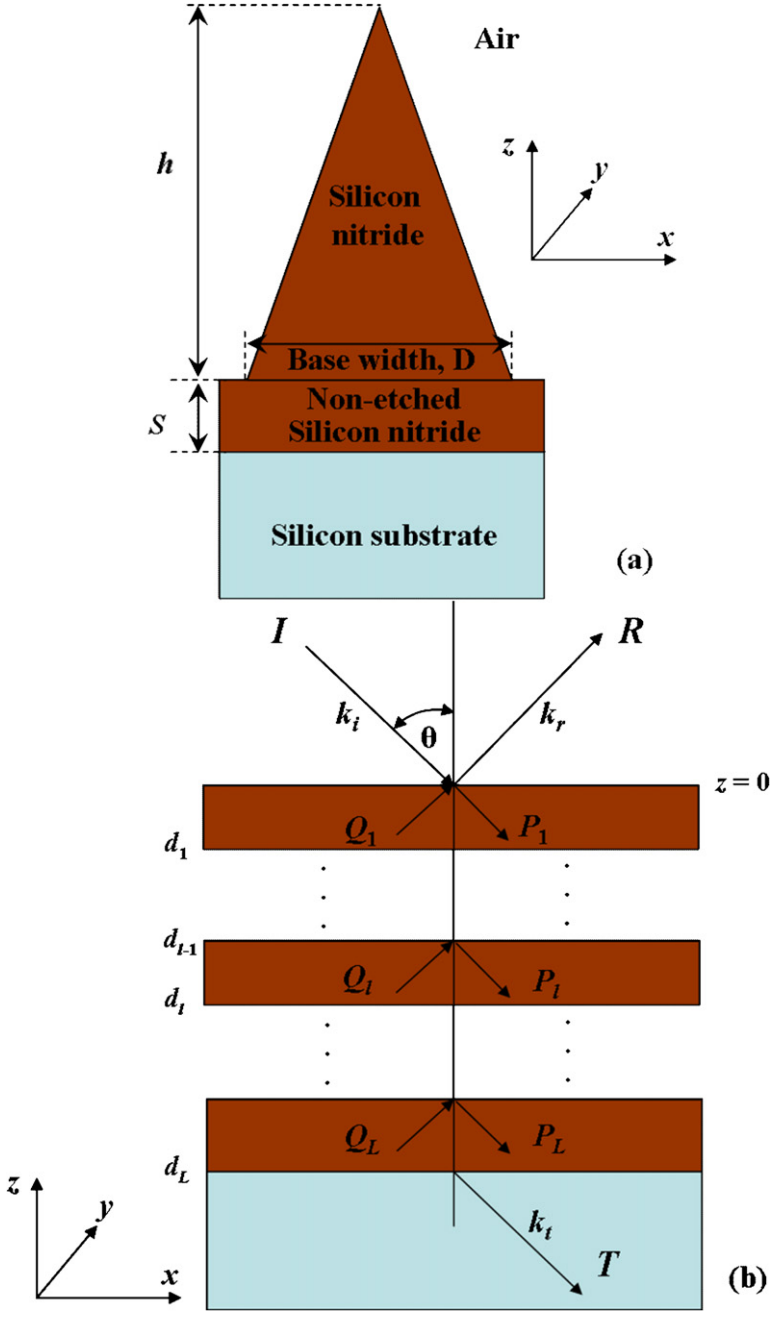

Fig. 1. (a) Geometry of sub-wavelength structure studied in this work, where h is the height and s is the non-etched part of SWS. (b) A stack of uniform homogeneous layers resulting from the partitioned geometry of (a) for the reflection calculation using the multilayer RCWA method and EMT. (For interpretation of the references to color in this figure, the reader is referred to the web version of this article.)

solution of Maxwell's equations for the electromagnetic diffraction by grating structures. A multilayer RCWA method is used in this study, where the effective medium theory (EMT) [23–25] is adopted to calculate the effective refractive index for each partitioned uniform homogeneous layer, as shown in Fig. 1(b).

Without loss of generality (WLOG), we first divide the pyramidal structure into several horizontal layers with equal thickness. As shown in Fig. 1(b), for each discrete position z_l along the z-direction, EMT implies that the effective refractive index $n(z_l)$ of each layer is approximated by

$$n(z_l) = \sqrt{\frac{[1 - f(z_l) + n_{\mathrm{SiN}}^2][f(z_l) + (1 - f(z_l))n_{\mathrm{SiN}}^2] + n_{\mathrm{SiN}}^2}{2[f(z_l) + (1 - f(z_l))n_{\mathrm{SiN}}^2]}}, \tag{1}$$

where $f(z_l) = 4r_l^2/\sqrt{3}D^2$ is the fraction of Si_3N_4 contained in each layer, r_l is the base width for each layer and D is the base width of the structure, $n_{\mathrm{SiN}} = n + ik$ is the complex refractive index of Si_3N_4, $i = \sqrt{-1}$, n and k are optical constants, and $n_{\mathrm{air}} = 1$ is the refractive index of air. Note that only the real part of refractive index of Si_3N_4 is considered in our simulation because it is weakly absorbing material [26]. With the calculated effective refractive index $n(z_l)$ for each layer, we can solve the reflectance property of the entire structure including a layer for the non-etched Si_3N_4 with respect to the different wavelength.

From the partitioned structure, shown in Fig. 1(b), we now consider the reflection and the transmission of a transverse electric (TE) polarized plane wave of free-space wavelength λ, incident at angle θ, on L uniform layers of effective refractive indices $n_1 = n(z_1), \ldots, n_l, \ldots, n_L = n(z_L)$ and thickness $d_1, \ldots, d_l, \ldots, d_L$. For each layer, the normalized electric field (in the x–y plane) for the input and the output regions is given by, for the air region, i.e., for $z \leqslant 0$

$$E_0 = \left(e^{-ik_{air,z}z} + R \times e^{-ik_{air,z}z}\right)e^{-ik_x x}, \tag{2}$$

for the region of SWS, i.e., for $D_{l-1} \leqslant z \leqslant D_l$,

$$E_l = \left(p_l \times e^{-ik_0\gamma_l(z-D_{l-1})} + Q_l \times e^{ik_0\gamma_l(z-D_l)}\right)e^{-ik_x x}, \tag{3}$$

and for the Si substrate, i.e., for $z \geqslant D_L$,

$$E_t = T \times e^{-i(k_x x + k_{Si,z}(z-D_L))}, \tag{4}$$

where

$$k_x = k_0 n_{\mathrm{air}} \sin\theta, \tag{5}$$

$$k_{\mathrm{air},z} = k_0 n_{\mathrm{air}} \cos\theta, \tag{6}$$

$$k_{\mathrm{Si},z} = k_0\sqrt{n_{\mathrm{Si}}^2 - n_{\mathrm{air}}^2 \sin^2\theta}, \tag{7}$$

$$\gamma_l = i\sqrt{n_l^2 - n_{\mathrm{air}}^2 \sin^2\theta}, \tag{8}$$

$$D_l = \sum_{p=1}^{l} d_p, \tag{9}$$

$l = 1, \ldots, L$, I, R and T are the incident, reflected and the transmitted amplitudes of the electric fields, P and Q are the field amplitudes in the uniform Si_3N_4 slab, $k_0 = 2\pi/\lambda$ is the wavevector magnitude, and $n$air and n_{Si} are the refractive indices of the air and the silicon regions. Note that now the layer of non-etched Si_3N_4 has been added into our simulation structure, where its effective refractive index $n_{\mathrm{SiN}} = 2.05$ is the same with the original one and $f(z_L) = 1$. The reflected and transmitted amplitudes of the explored SWS are calculated by matching the tangential electric- and magnetic-field components at the boundaries among layers [27]. First, for the boundary between the input air region and the first layer of Si_3N_4 (i.e., $z = 0$), we have

$$\begin{cases} 1 + R = P_1 + Q_1 \times e^{-k_0\gamma_1 d_1}, \\ i\frac{k_{\mathrm{air},z}}{k_0}(1 - R) = \gamma_1(P_1 - Q_1 \times e^{-k_0\gamma_1 d_1}). \end{cases} \tag{10}$$

For the boundary between the $(l-1)$st and the lth layers (i.e., $z = D_{l-1}$)

$$\begin{cases} P_{l-1} \times e^{-k_0\gamma_{l-1}d_{l-1}} + Q_{l-1} = P_l + Q_l \times e^{-k_0\gamma_l d_l}, \\ \gamma_{l-1}(P_{l-1} \times e^{-k_0\gamma_{l-1}d_{l-1}} - Q_{l-1}) = \gamma_l(P_l - Q_l \times e^{-k_0\gamma_l d_l}); \end{cases} \tag{11}$$

for the boundary between the last layer and the output Si region (i.e., $z = D_L$), the matched equations are

$$\begin{cases} P_L \times e^{-k_0\gamma_L d_L} + Q_L = T, \\ \gamma_L(P_L \times e^{-k_0\gamma_L d_L} - Q_L) = i(\frac{k_{\mathrm{Si},z}}{k_0})T. \end{cases} \tag{12}$$

Eqs. (10)–(12) could be solved by using a transmittance matrix method [28]. Using Eq. (12), the field amplitudes P_L and Q_L in terms of the transmitted coefficient T are determined firstly. They are then substituted into Eq. (11) for the field amplitudes P_{L-1} and Q_{L-1}. Consequently, the system of equations to be solved for the reflection properties is given by

$$\begin{aligned} &\begin{bmatrix} 1 \\ i\frac{k_{\mathrm{air},z}}{k_0} \end{bmatrix} + \begin{bmatrix} 1 \\ -i\frac{k_{\mathrm{air},z}}{k_0} \end{bmatrix} R \\ &= \prod_{l=1}^{L} \begin{bmatrix} 1 & e^{-k_0\gamma_l d_l} \\ \gamma_l & -\gamma_l e^{-k_0\gamma_l d_l} \end{bmatrix} \\ &\quad \times \left[\begin{pmatrix} e^{-k_0\gamma_l d_l} & 1 \\ \gamma_l e^{-k_0\gamma_l d_l} & -\gamma_l \end{pmatrix} \right]^{-1} \times \begin{bmatrix} 1 \\ i\frac{k_{\mathrm{Si},z}}{k_0} \end{bmatrix} T, \end{aligned} \tag{13}$$

for partitioned layers of SWS. Similarly, a set of governing equations could be derived for the transverse magnetic (TM) polarization. Here the incident angle θ of sun light is assumed to be normal to the plane (i.e., $\theta = 0°$), and only the TE polarization is considered here for the calculation of the reflection properties [29].

For a given number of layers for the SWS including the layer of non-etched Si_3N_4, say L in total; a calculation procedure for computing the reflectance properties of the studied SWS described above is summarized: (i) calculate the effective refractive index for each z_l via Eq. (1); (ii) compute the coefficients using Eqs. (5)–(9) for a specified wavelength λ; and (iii) solve Eq. (13) to get the unknowns R and T.

The reflectance spectra obtained from RCWA simulation above are used in PC1D simulation to compare the effect on the short circuit current density (J_{SC}), open circuit voltage (V_{OC}) and efficiency (η) for a solar cell structure.

3. Results and discussion

First of all, we compare the reflectance with respect to the wavelength of sunlight for the SWS with Si and Si_3N_4. As shown in Fig. 2, by assuming a constant refractive index for Si $n_{\mathrm{Si}} = 3.875$ and for Si_3N_4 $n_{\mathrm{SiN}} = 2.05$, the reflectance versus the wavelength for Si SWS with $h = 88$ nm and Si_3N_4 SWS with $h = 88$ nm and vanished non-etched part of SWS (i.e., $s = 0$ nm) is simulated and compared. It is found that the non-optimized Si_3N_4 SWS possesses a little bit higher reflectance which may not be a plus for ARC. However, we can design a Si_3N_4 SWS with the case of non-zero s, say $h = 68$ nm and $s = 20$ nm, which shows that the reflectance is close to the result of Si SWS or even better. This observation motivates us to explore the morphology-dependent reflectance of Si_3N_4 SWS with a set of optimized h and s. Note that Si refractive index n_{Si} may depend upon the wavelength of incident sunlight [30]; our calculation for the Si_3N_4 SWS with $h = 68$ nm and $s = 20$ nm confirms the reflectance difference between the model with constant and wavelength-dependent n_{Si}, as shown in Fig. 3. In this calculation, an empirically fitted formula for the wavelength-dependent n_{Si} is implemented in our simulation program [31]

$$n_{\mathrm{Si}} = \sqrt{\varepsilon + \frac{A}{\lambda^2} + \frac{B\lambda_1^2}{(\lambda^2 - \lambda_1^2)}}, \tag{14}$$

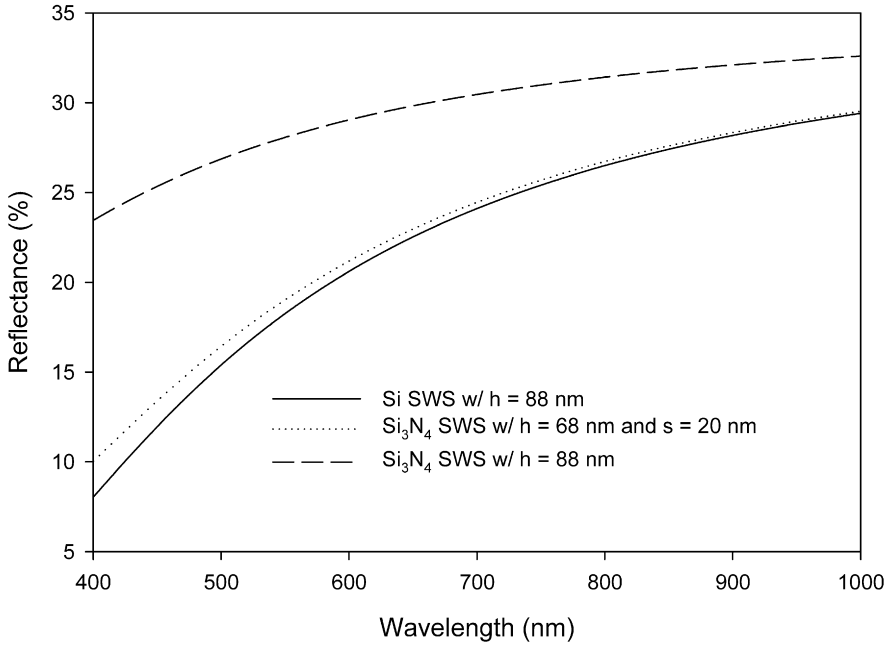

Fig. 2. The reflectance versus the wavelength for Si SWS with $h = 88$ nm and Si_3N_4 SWS with $h = 88$ nm and vanished non-etched part of SWS (i.e., $s = 0$ nm). Comparison for the Si_3N_4 SWS with the case of non-zero s, say $s = 20$ nm is also provided. It is found that it is possible to reduce the reflectance of Si_3N_4 SWS by proper selection of h and s.

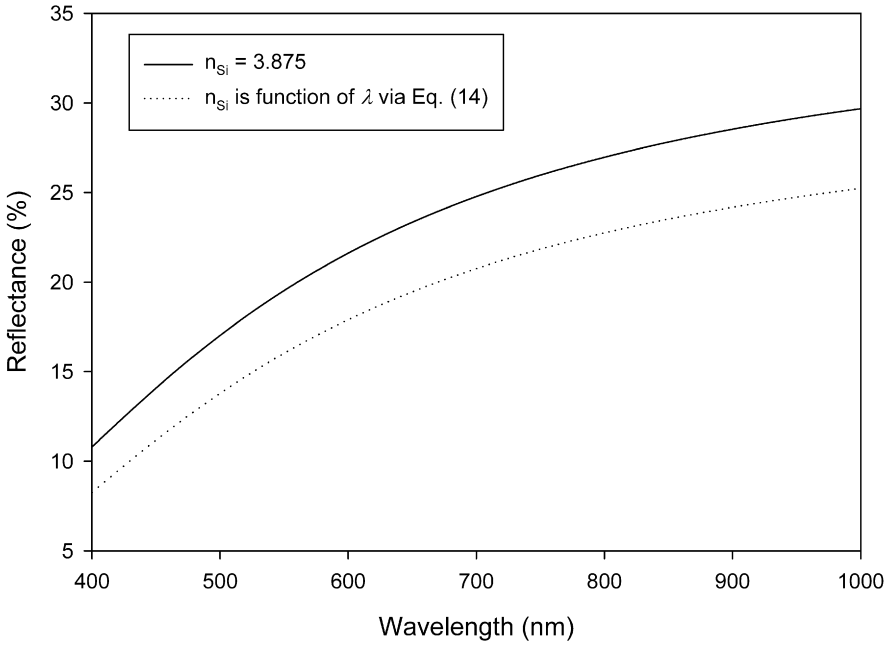

Fig. 3. The spectral reflectivity of Si_3N_4 SWS for $h = 68$ nm and $s = 20$ nm with constant Si refractive index and refractive index as a function of lambda given by Eq. (14).

where, $\lambda_1 = 1.1071$ μm, $\varepsilon = 11.6858$, $A = 0.939816$ and $B = 8.10461 \times 10^{-3}$.

Instead of considering the reflectance for a certain wavelength, an effective reflectance is further computed for the structures over a range of the wavelength of incident sunlight. By taking purely Si in the SWS part of Fig. 1(a), where $s = 0$ nm and h is designed as a varying factor, we now calculate the effective reflectance R_{eff} [32] for the wavelength λ varying from $\lambda_l = 400$ nm to $\lambda_u = 1000$ nm and compare it with Si_3N_4 SWS. R_{eff} is evaluated by

$$R_{eff} = \frac{\int_{\lambda_l}^{\lambda_u} \frac{R(\lambda)SI(\lambda)}{E(\lambda)}\, d\lambda}{\int_{\lambda_l}^{\lambda_u} \frac{SI(\lambda)}{E(\lambda)}\, d\lambda}, \tag{15}$$

where, $SI(\lambda)$ is spectral irradiance given by ATMG173 AM1.5G reference [33], $E(\lambda)$ is photon energy and $R(\lambda)$ is the calculated reflection. Figs. 4(a) and 4(b) show the effective reflectance as a function of h for Si SWS, and of h and s for Si_3N_4 SWS. For Si SWS, there is a minimum $R_{eff} = 3.89\%$ for $h = 220$ nm, and for Si_3N_4 SWS, the minimum of $R_{eff} = 1.77\%$ occurs at $h = 150$ nm and $s = 70$ nm. Compared with Si SWS, the twice improvement of R_{eff} for Si_3N_4 SWS is due to the nature of Si_3N_4 and an optimal combination of the height of etched part of Si_3N_4 and the thickness of non-etched part of Si_3N_4.

It has been reported that SLAR and DLAR were used in solar cell, for a unified comparison, similarly, we further examine their R_{eff} over the same wavelength, as shown in Figs. 5(a) and 5(b).

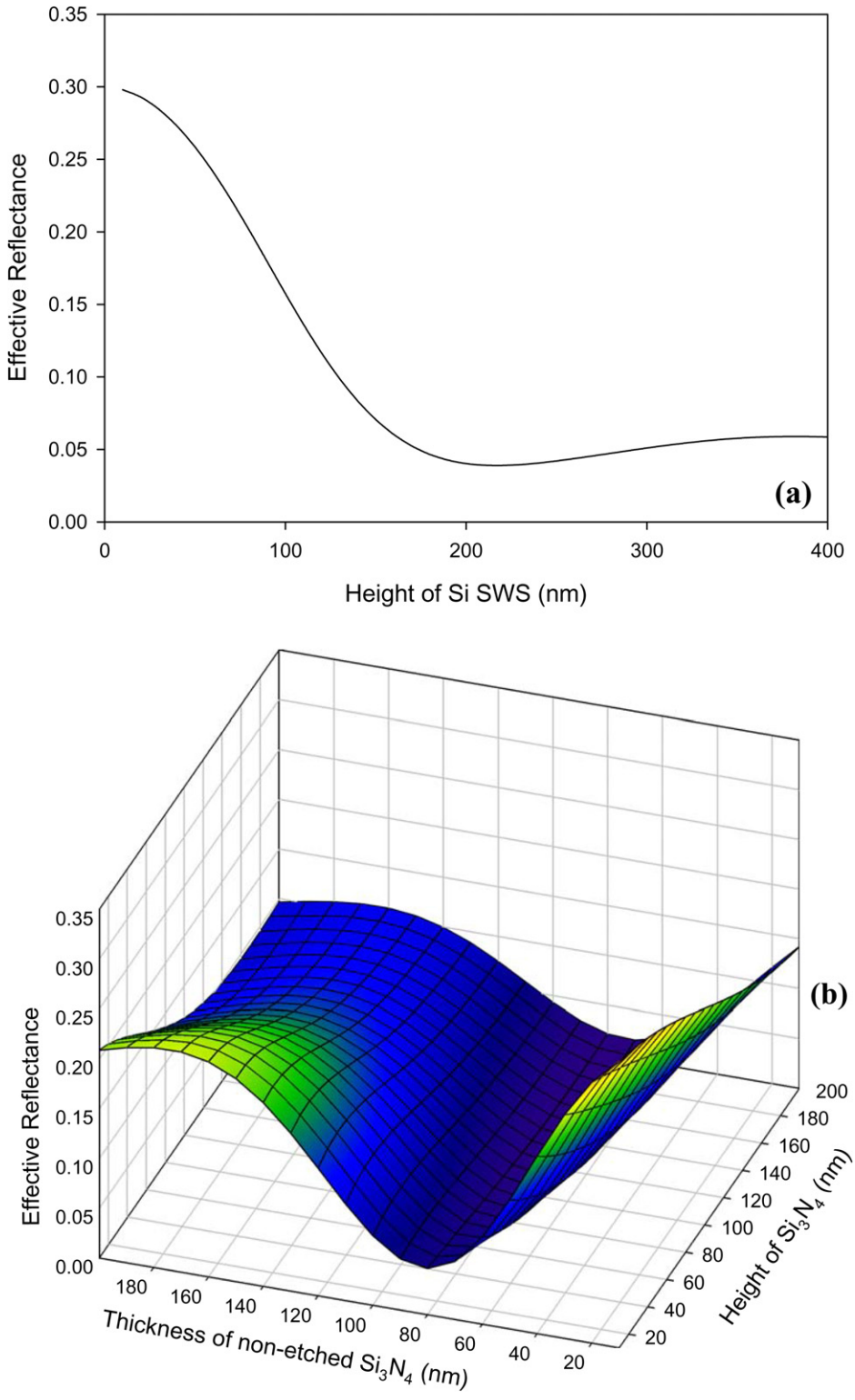

Fig. 4. The effective reflectance for the wavelength varying from 400 to 1000 nm; plot is as a function of (a) h for Si SWS and (b) of h and s for Si_3N_4 SWS.

For Si_3N_4 SLAR coating on Si, as shown in the inset of Fig. 5(a), the refractive index is equal to 2.05, where the thickness of ARC is varied. For Si_3N_4/ARC 2 DLAR coating on Si, the thickness of ARC 2 and the refractive index of ARC 2 are varied. Note that the thickness of ARC 1 equals 80 nm, as shown in the inset of Fig. 5(b), directly comes from the optimal value of Fig. 5(a), and the lower bound of refractive index of ARC 2 starts from 1.38 which is the refractive index of MgF_2. The lowest R_{eff} occurs when the refractive index of ARC 2 is 1.38 and its thickness is 100 nm.

Based upon the investigation of Figs. 4 and 5, we show the optimal reflectance spectra among the bulk Si (i.e., the bare Si), the optimized SLAR, DLAR, Si SWS and Si_3N_4 SWS for the wavelength from 400 to 1000 nm in Fig. 6. Table 1 lists the effective reflectivity for those optimized structures of 150 nm Si_3N_4 SWS and 70 nm non-textured Si_3N_4 film, com-

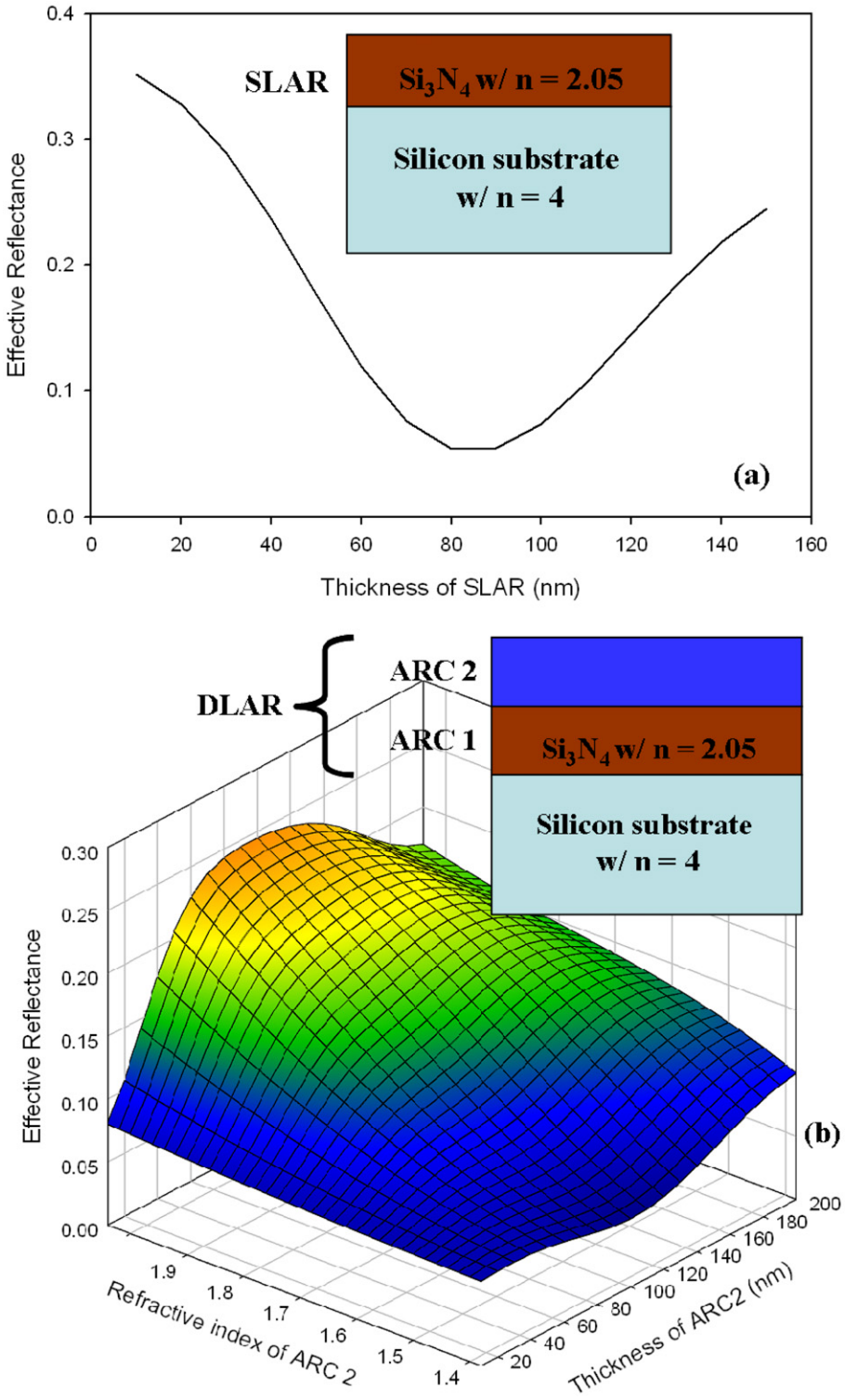

Fig. 5. Plot of the effective reflectance for the wavelength varying from 400 to 1000 nm. (a) is the result as a function of the thickness of Si_3N_4 ARC with $n = 2.05$ for SLAR coating on Si. (b) is the result as a function of the thickness of ARC 2 and refractive index of ARC 2 for Si_3N_4/ARC_2 DLAR coating on Si. The thickness of Si_3N_4 ARC 1 is fixed at 80 nm which is optimized from (a).

pared with the Si SWS, Si_3N_4 SLAR (its thickness is 80 nm) and Si_3N_4/MgF_2 DLAR (its thickness is 80–100 nm) structures. The flat silicon substrate exhibits high reflection >35% for visible and near infrared wavelengths, Si_3N_4 SLAR coatings exhibits low reflection <20% for long wavelengths 700 nm and high reflection >35% for shorter wavelengths 400 nm, and Si_3N_4/MgF_2 DLAR coatings exhibits low reflection <10% for long wavelengths 700 nm and high reflection >20% for short wavelength 400 nm, while the SWS gratings show reduced reflection of <10% for whole wavelengths. The Si_3N_4 SWS with $h = 150$ nm and $s = 70$ nm exhibits lowest effective reflectivity among five structures; consequently, the optimized morphology of Si_3N_4 SWS could be a promising alternative for DLAR in Si solar cell technology.

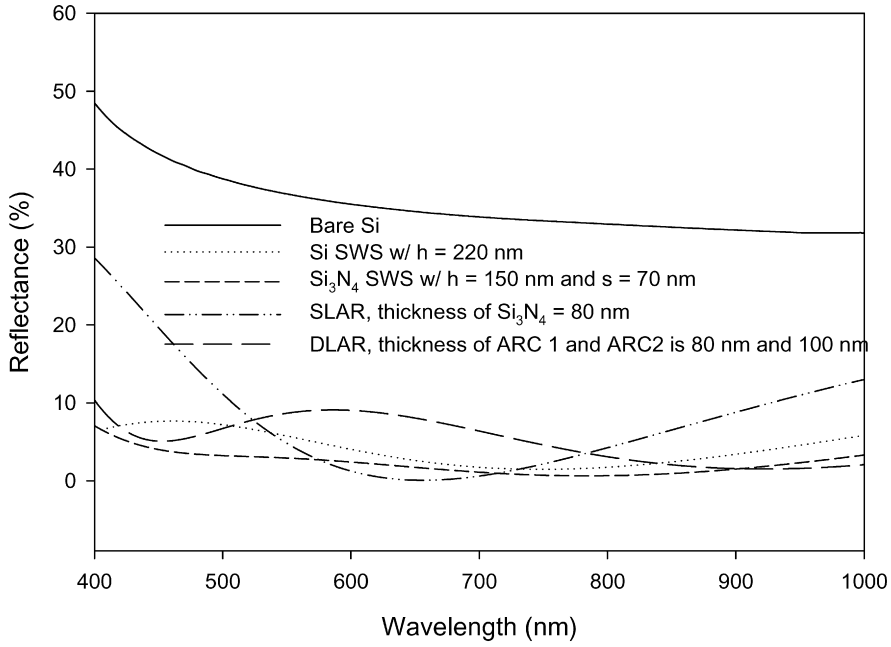

Fig. 6. Comparison of the reflectance spectra among the bulk Si (i.e., the bare Si), the optimized SLAR, DLAR, Si SWS and Si_3N_4 SWS for the wavelength from 400 to 1000 nm.

Table 1
Effective reflectivity for those optimized structures of 150 nm Si_3N_4 SWS and 70 nm non-textured Si_3N_4 film, compared with the Si SWS, Si_3N_4 SLAR (its thickness is 80 nm) and Si_3N_4/magnesium fluoride DLAR (its thickness is 80–100 nm) structures.

ARC structure	R_{eff} (%) for $\lambda = 400$–1000 nm
Si_3N_4 SWS	1.77
Si SWS	3.89
DLAR	5.39
SLAR	5.41

The reflectance spectra are used as the input of PC1D to compare the effect on J_{SC}, V_{OC} and η for a solar cell structure. In the simulation, p-type Si is set with resistively of 1.008 Ω cm and a diffused emitter with error function distribution, where the emitter sheet resistance is 99.4 Ω/sq. The base contact resistance is 0.015 Ω and the cell's internal shunt conductance is 0.3 Siemens. The bulk life time of Si is set to 7.03 μs, where the front and back surface recombination velocity is 1800 and 25 cm/s, respectively [34]. Electrical characteristics and the external quantum efficiency obtained from PC1D simulation for a Si solar cell using the reflectance spectra for the three explored structures, they are Si_3N_4 SWS, SLAR and DLAR are further conducted as shown in Fig. 7. It is clear that J_{SC} and V_{OC} of Si_3N_4 SWS are higher than those of Si_3N_4 SLAR and Si_3N_4/MgF_2 DLAR structures, as seen from Fig. 7(a). A clear increase in efficiency of 1% can be seen for silicon solar cell with Si_3N_4 SWS over a cell with single layer Si_3N_4 ARCs and 0.71% higher in efficiency than the DLAR coated solar cell, which is due to lower reflectance of DLAR to Si_3N_4 SWS over the longer wavelength region that leads to lower short circuit current.

With solar cells, the external quantum efficiency is often measured, which could be calculated by the current obtained outside the device per incoming photon. As shown in Fig. 7(b), the calculated external quantum efficiency also confirms the higher efficiency of the designed Si_3N_4 SWS compared with the others. For the short and long wavelengths, the low external quantum efficiency observed in Si_3N_4 SLAR is mainly from higher reflectance (see the dash-dot-dot line of Fig. 6). We believe that Si_3N_4 SWS gratings exhibit lower reflection than colloid-based antireflection coatings on crystalline silicon solar cells, which is now under our fabrication study.

4. Conclusions

In this paper, we have presented preliminary results of designed silicon nitride sub-wavelength structures. Using the results of rigorous coupled wave analysis simulation for the pyramidal-shaped silicon nitride sub-wavelength structures, the ratio of silicon nitride sub-wavelength structures height and non-textured part of silicon nitride has been optimized. The reflectance results for the optimized sub-wavelength structures have been compared in terms of effective reflectivity. Then lowest effective reflectivity sub-wavelength structures were compared with previously optimized 80 nm Si_3N_4 SLAR and 80/100 [nm/nm] Si_3N_4/MgF_2 DLAR. A low effective reflectivity of 1.77% can be obtained for a silicon nitride SWS height and non-etched layer of 150 and 70 nm respectively, which is less than 80 nm Si_3N_4 SLAR of 5.41% and comparable with Si_3N_4/MgF_2 DLAR of 5.39%. The solar cell efficiency results obtained from PC1D using the reflectance data obtained from RCWA simulation shows the clear increase of 1% for SWS as compared with SLAR. Based upon our theoretical investigation, we are currently fabricating the optimized silicon nitride sub-wavelength structures for solar cells. In addition, there is a need to study more about fabrication of silicon nitride sub-wavelength structure to improve the solar cell efficiency with a single layer ARCs which is believed to reduce the reflectance and improve the passivation properties of silicon solar cell.

Acknowledgements

This work was supported in part by Taiwan National Science Council (NSC) under Contracts NSC-97-2221-E-009-154-MY2, NSC-97-2752-E-009-001-PAE and by Motech Industries Inc. (MOTECH), Tainan, Taiwan, under a 2008–2009 grant.

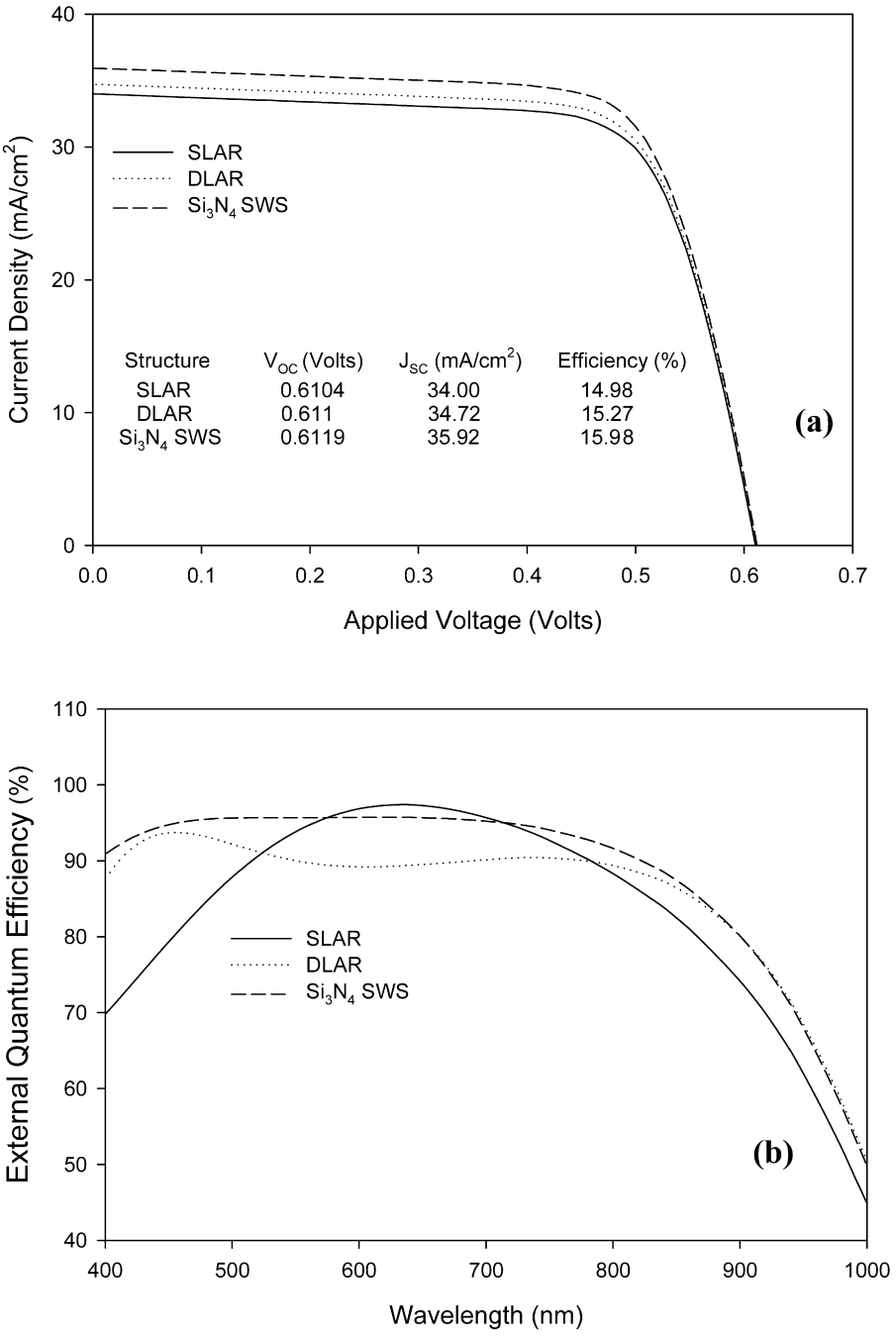

Fig. 7. (a) Electrical characteristics and (b) the external quantum efficiency obtained from PC1D simulation for a silicon solar cell using the reflectance spectra for the three optimized structures, they are Si_3N_4 SWS, SLAR and DLAR.

References

[1] M.A. Green, High Efficiency Silicon Solar Cells, Trans Tech Publication, Aedermannsdorf, 1987.

[2] S.M. Sze, Semiconductor Devices, Physics and Technology, Wiley, New York, 1985.

[3] Strehlke, S. Bastide, J. Guillet, C. Levy-Clement, Mat. Sci. Eng. B 69 (2000) 81–86.

[4] S.Y. Lien, D.S. Wuu, W.C. Yeh, J.C. Liu, Sol. Energy Mater. Sol. Cells 90 (2006) 2710–2719.

[5] S.K. Dhungel, J. Yoo, K. Kim, S. Jung, S. Ghosh, J. Yi, J. Korean Phys. Soc. 49 (2006) 885–889.

[6] V.M. Aroutiounian, K. Martirosyan, P. Soukiassian, J. Phys. D: Appl. Phys. 39 (2006) 1623–1625.

[7] B.S. Richards, S.F. Rowlands, C.B. Honsberg, J.E. Cotter, Prog. Photovolt: Res. Appl. 11 (2003) 27–32.

[8] M.F. Schubert, F.W. Mont, S. Chhajed, D.J. Poxson, J.K. Kim, E.F. Schubert, Opt. Express 16 (2008) 5290–5298.

[9] P. Lalanne, G.M. Morris, Nanotechnology 8 (1997) 53–56.

[10] Y.C. Chang, G.H. Mei, T.W. Chang, T.J. Wang, D.Z. Lin, C.K. Lee, Nanotechnology 18 (2007) 285–303.

[11] M.J. Minot, J. Opt. Soc. Am. 66 (1976) 515–519.

[12] T. Glaser, A. Ihring, W. Morgenroth, N. Seifert, S. Schröter, V. Baier, Microsystem Technologies 11 (2005) 86–90.

[13] K. Hadobas, S. Kirsch, A. Karl, M. Acet, E.F. Wassermann, Nanotechnology 11 (2000) 161–164.

[14] Y. Kanamori, M. Sasaki, K. Hane, Opt. Lett. 24 (1999) 1422–1424.

[15] Z.N. Yu, H. Gao, W. Wu, H.X. Ge, S.Y. Chou, J. Vac. Sci. Technol. B 21 (2003) 2874–2877.

[16] H. Sai, H. Fujii, K. Arafune, Y. Ohshita, M. Yamaguchi, Y. Kanamori, H. Yugami, Appl. Phys. Lett. 88 (2006) 20116–20118.

[17] Y. Inomata, Sol. Energy Mater. Solar Cells 48 (1997) 237–242.
[18] H.F.W. Dekkers, Opto-Elctron. Rev. 8 (2000) 311–316.
[19] M.G. Moharam, T.K. Gaylord, J. Opt. Soc. Am. 71 (1981) 811–818.
[20] M.G. Moharam, T.K. Gaylord, J. Opt. Soc. Am. A 3 (1986) 1780–1787.
[21] M.G. Moharam, D.A. Pommet, J. Opt. Soc. Am. A 12 (1995) 1077–1086.
[22] D.A. Clugston, P.A. Basore, in: Proc. the 26th IEEE Photovoltiac Specialists Conf., Anaheim, 1997, pp. 207–210.
[23] L. Lalanne, M. Hutley, Artificial Media Optical Properties-Subwavelength Scale Encyclopedia of Optical Engineering, Dekker, New York, 2003.
[24] P. Yeh, Optical Waves in Layered Media, Wiley, New York, 1991.
[25] D.A.G. Bruggeman, Ann. Phys. 24 (1935) 636–679.
[26] J. Zhao, M.A. Green, IEEE Trans. Electron Dev. 38 (1991) 1925–1934.
[27] H.A. Macleod, Thin-Film Optical Filters, 3rd ed., Institute of Physics, Bristol, 2001.
[28] L.M. Brekhovshikh, Waves in Layered Media, Academic, New York, 1960.
[29] K.L. Chopra, S.R. Das, Thin Film Solar Cells, Plenum Press, New York, London, 1983.
[30] C.-H. Sun, W.-L. Min, N.C. Linn, P. Jiang, Appl. Phys. Lett. 91 (2007) 231105–231107.
[31] S. Khedim, A. Chiali, B. Benyoucef, N.E. Chabane Sari, in: Proc. Revue des Energies Renouvelables ICRESD-07, Tlemcen, 2007, pp. 337–341.
[32] D.N. Wright, E.S. Marstein, A. Holt, in: Proc. the 31st IEEE Photovoltiac Specialists Conf., Orlando FL, 2005, pp. 1237–1240.
[33] http://rredc.nrel.gov/solar/spectra/am1.5/ASTMG173.html.
[34] http://www.semiconductor.net/article/CA6572786.html.